Energy materials

The effect of oxidative functionalization of carbon nanotubes on the morphological, optical, and photoelectrochemical properties of modified titanium dioxide photoanodes

Francisco J. Peón-Díaz[1,2], Rodrigo Segura del Río[1,*] ⓘ, Samuel Hevia[3], Fernanda Olivares[4],
Juan Carlos Expósito-Gálvez[5], Renán Escalante[5], Karen Valadez-Villalobos[5],
Antonio J. Riquelme[5], Gerko Oskam[5,6], and Ricardo Henríquez[4]

[1] *Instituto de Química y Bioquímica, Facultad de Ciencias, Universidad de Valparaíso, Gran Bretaña 1111, 2360102 Valparaíso, Chile*

[2] *Programa Conjunto de Doctorado en Ciencias Mención Química, Universidad Técnica Federico Santa María – Universidad de Valparaíso, Valparaíso, Chile*

[3] *Instituto de Física, Facultad de Ciencias, Pontificia Universidad Católica de Chile, Santiago de Chile, Chile*

[4] *Departamento de Física, Universidad Técnica Federico Santa María, Valparaíso, Chile*

[5] *Department of Physical, Chemical and Natural Systems, Universidad Pablo de Olavide, 41013 Seville, Spain*

[6] *Department of Applied Physics, CINVESTAV-IPN, 97310 Mérida, Yucatán, Mexico*

ABSTRACT

In this work, we demonstrate the influence of the oxidative treatment of carbon nanotubes (CNTs) on the morphological, optical, and photoelectrochemical properties of CNTs-TiO$_2$ photoanodes. CNTs were synthesized by a chemical vapor deposition method (CVD) and subsequently oxidized in a mixture of HNO$_3$/H$_2$SO$_4$ to introduce nitrogen- and oxygen-containing functional groups. The oxidation time was varied (45, 90, and 180 min) to obtain CNTs with different oxidation levels (CNTs-ox). Pristine and oxidized CNTs were deposited on ITO and used as substrates to fabricate ITO/CNTs/TiO$_2$ photoelectrodes by depositing a TiO$_2$ thin layer using a CVD procedure. The extent of oxidation of the CNTs was found to directly influence the homogeneity and morphology of the TiO$_2$ overlayer, its physical stability, and the optical and photoelectrochemical properties of the photoelectrodes. An optimum oxidative treatment was achieved for 90 min, leading to a CNTs-ox/TiO$_2$ electrode with the best performance. Compared to shorter and longer times, this sample showed the smallest bandgap and the best homogeneity of TiO$_2$ growth on the CNTs' surface. Optimal photoelectrochemical performance was also found for this sample (160 μA/cm^2 at 0 V vs. Ag/AgCl) in KCl (0.1 M) electrolyte (100 mW/cm^2, Xenon arc lamp).

GRAPHICAL ABSTRACT
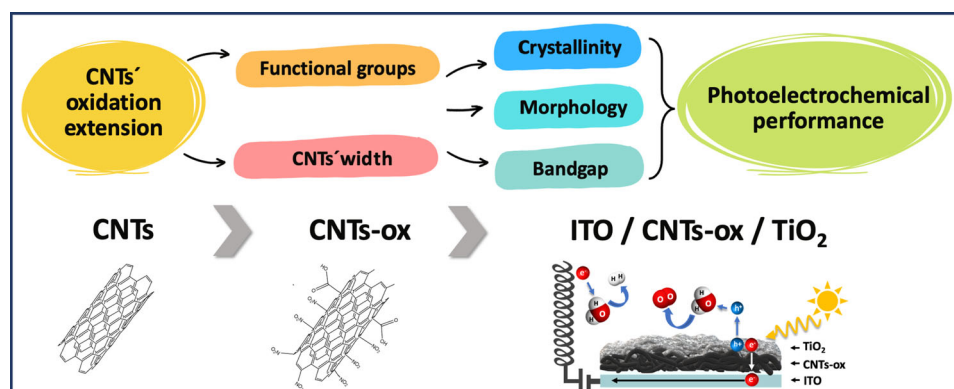
Introduction

The production of green hydrogen from water splitting is a topic that has received increasing attention in the last few decades [1]. Specifically, the photoelectrochemical (PEC) strategy is a promising approach for this purpose due to the possibility of generating H_2 (separately from O_2) directly from sunlight in a single device [2]. Nevertheless, several issues must still be addressed regarding the semiconductor materials (SCs) to achieve an optimal balance of light absorption and charge transfer and minimize electron–hole recombination processes [3].

Numerous strategies have been proposed in this sense, including morphology modulation to increase surface area [4]. This increases active sites in the SC, allowing better charge transfer to the electrolyte. To improve photon harvesting, SCs have been sensitized with dyes [5–7], quantum dots [8–15], or plasmonic materials [16–23], broadening light absorption into the visible region and allowing enhanced photoelectrochemical performance. Furthermore, combining SCs and carbonaceous nanomaterials composites has also been proposed to increase charge separation, free carrier mobility, and long-term stability [24, 25]. The most common materials in this sense are graphene and graphene oxides [26–30], carbon nitrides [31–34], and carbon nanotubes [28, 35–37].

Among them, carbon nanotubes (CNTs) stand due to their easiness of fabrication, high conductivity, and the elevated surface-to-mass ratio [25]. CNTs show extended conductivity along the tube axis due to long-range π conjugation; hence, when combined with SCs, they allow for fast harvesting and separation of photogenerated charges [24]. Also, an increase in charge carrier density has been reported in CNTs-SCs photoelectrodes compared with bare SCs [38]. Furthermore, when CNTs are used as substrates for SC materials in sandwich-like photoelectrodes, they modulate the morphology, grain size, and structure of the SCs.

Among CNTs-SCs composites, titanium dioxide-based materials have received attention in the last decade for water-splitting applications. Hierarchical CNTs-TiO$_2$ hybrid structures show an increased surface area, more reactive sites, and superior electrochemical performance [39, 40]. Studies in this direction have shown the importance of controlling the CNTs ratio [41], the previous functionalization of CNTs [42], and the synthetic method chosen for preparing the composite [43–45].

Functionalizing CNTs is a widespread approach when fabricating CNTs composites. It increases their dispersibility in solvents and favors their covalent interactions with other materials, as is the case for SCs [46]. The first is relevant, considering that most of the preparation methods are carried out in solution or including the dispersion of CNTs. The second allows

for better attachment of both materials, crucial for charge transfer kinetics optimization [24].

HNO_3 and HNO_3-H_2SO_4 or H_2SO_4-H_2O_2 mixtures have been used as oxidative agents, and an extensive discussion has been reported in the literature on the structural and chemical modification of CNTs after these treatments [47–49]. Nevertheless, most reports in this sense relate to the functionalization with oxygenated groups (C=O, C–OH, OCO; COOH), and only a few [50, 51] have paid attention to the introduction of nitrogen in CNTs as a dopant or in functional groups as amide or nitro moieties.

In a recent article from our group, we found that functionalizing CNTs with nitrogen and oxygen-containing groups was crucial to enhancing the photoconversion efficiency of CNTs-TiO_2 photoanodes fabricated by chemical vapor deposition [52]. Also, other reports have shown that introducing nitrogen in CNTs improves electrocatalytic and photocatalytic performance in several CNTs-SCs composites [42]. Nevertheless, despite the oxidation of carbon nanotubes being a well-covered area, more attention should be given to the effect of the oxidation of CNTs on the morphological, optical, and electrochemical performance of hybrid photoelectrodes. Here, we present a comprehensive study concerning the functionalization of CNTs to understand the influence on the formation of CNTs-TiO_2 nanostructures. The result of CNTs oxidation on the morphological, structural, and optical properties of CNTs-TiO_2 films is discussed, and its effect on the photoelectrochemical performance of the photoanodes is demonstrated and analyzed.

Methods

Preparation of CNTs-ox

In the first step, multi-walled carbon nanotubes (CNTs) were synthesized in a CVD furnace using Pd (2%)/Al_2O_3 [53] as a catalyst and acetylene as a carbon source. This synthesis method was previously reported by our group [54]. Then as-prepared CNTs were further purified (in 3 M HCl for 24 h., and after in 5% NaOH for 24 h.), rinsed until neutral pH was attained, and dried overnight at 60 °C to obtain pristine carbon nanotubes **(CNTs-Pri)**.

Secondly, an oxidative treatment was performed using a mixture of HNO_3/H_2SO_4 (9/10 (v/v))

following a previously reported method [50]. Briefly, 25 mg of CNTs were dispersed in 2.85 mL of the acid mixture, sonicated for 5 min, and then heated to 60 °C with continuous stirring. This temperature is optimum to achieve -NO_2 groups on the CNT surface [50]. Three reaction times were used: 45, 90, and 180 min to obtain oxidized CNTs denoted as **CNTs-ox-45**, **CNTs-ox-90**, and **CNTs-ox-180**, respectively (see Fig. 1).

Various analysis methods were performed to understand the effect of oxidation on the structural properties of CNTs, as well as the presence of functional groups and defects: transmission electron microscopy (JEOL 1320, 80 kV), Fourier-transform infrared spectroscopy (FT-IR) (Thermo Scientific-Nicolet IS10.), X-ray photoelectron spectroscopy (XPS) (Staib Surface Analysis Station 1 for AES and XPS analysis), and Raman spectroscopy (Renishaw-inVia, 532 nm laser).

CNTs/TiO_2 photoelectrode fabrication and characterization

The photoanodes were prepared using the same method reported previously by our group [52]. In a standard procedure, CNTs-X (being X: Pri, ox-45, ox-90, and ox-180) were dispersed in 2-propanol and drop-casted onto indium tin oxide (ITO) substrates (7 Ω/cm^2). Then, ITO/CNTs substrates were introduced into a two-zone CVD furnace, and TiO_2 was grown at 500 °C using titanium isopropoxide (TTIP–Sigma Aldrich, 97%) as a precursor and 30 min as reaction time (see Fig. 1).

The films were characterized by Scanning Electron Microscopy (ESEM Quattro S-Thermo Fisher Scientific), Diffuse Reflectance (Shimadzu UV 2600), Raman (Renishaw-inVia, 532 nm laser), and X-Ray Diffraction (XRD) (Bruker D8 Discover) analysis.

Photoelectrochemical measurements were conducted in a three-electrode cell using an Ag/AgCl (1 M) reference electrode, Pt wire as the counter electrode, and KCl (0.1 M) as electrolyte. A 300W Xenon arc-lamp (100 mW cm^{-2}) was used as a light source, and a potentiostat (Gamry Instrument, Interface 1000) was employed to conduct open circuit potential (OCP) measurements, linear sweep voltamperometry (LSV), and chronoamperometry measurements.
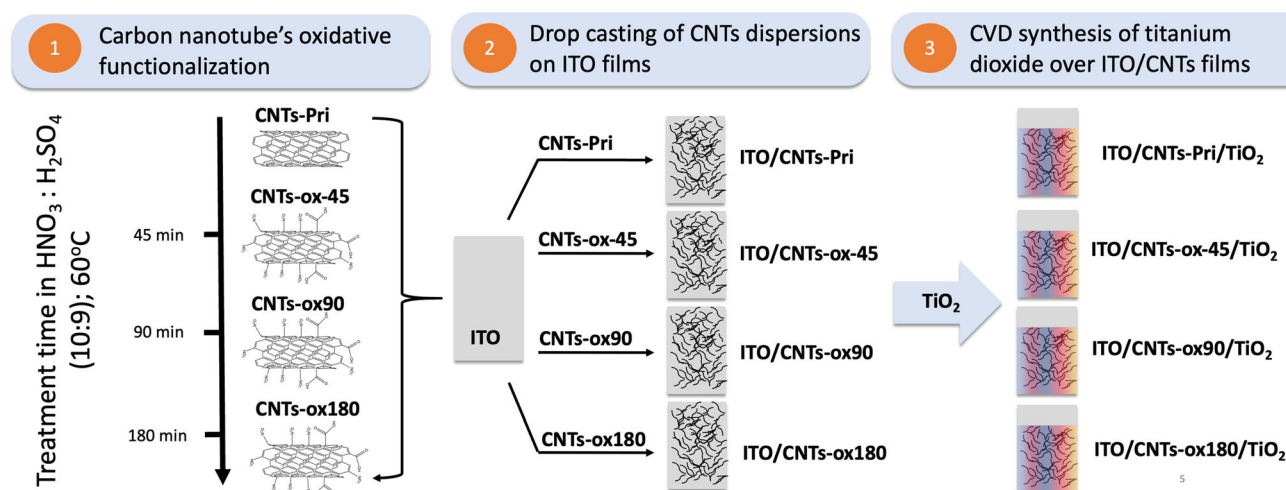
Figure 1 Schematics of the preparation procedure of (1) CNTs functionalized at different oxidation times, (2) drop-casting of CNTs on ITO films, and (3) TiO$_2$ deposition by CVD over the ITO/CNTs films.

Results and discussion

CNTs: functionalization and structure

Figure 2 shows the FT-IR spectra of the carbon nanotubes, both untreated (CNTs-Pri) and oxidized (CNTs-ox: with 45, 90, and 180 corresponding to the oxidation time in minutes). All CNTs-ox samples show the presence of signals corresponding to nitrogen and oxygen-containing functional groups (signals of –NH$_2$ at 3728 cm^{-1}, –NO$_2$ at 1380 cm^{-1} and 1450 cm^{-1}, O–H at 3440 cm^{-1}, C=O at 1720 cm^{-1}, and C–O at 1100 cm^{-1}).
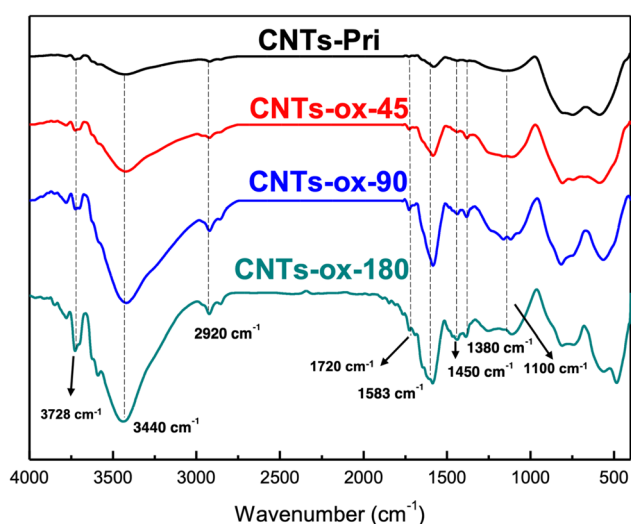

Figure 2 FT-IR spectra of pristine carbon nanotubes (black line) and CNTs oxidized at various extensions: 45 min (red line), 90 min (blue line), and 180 min (green line).

Specifically, the presence of –NO$_2$ groups increases for longer oxidation times, which can be corroborated by the observed enhancement of the FT-IR signals corresponding to the symmetric and asymmetric vibrations of –NO$_2$ groups at 1380 and 1450 cm^{-1} [55]. Also, oxygen-containing functional groups increased with the extent of oxidation, similar to previous reports where similar oxidative conditions have been used [47, 49].

To gain a better understanding of the nature of the functionalization of CNTs, X-ray photoelectron spectroscopy (XPS) was carried out. The broad range XPS spectra can be found in the Supplementary Information (Figure S1). Figure 3a shows the deconvolution of the C1s signal for the four CNTs synthesized. In all cases, the typical signals of C–C sp2 (284.4 eV) and C–C sp3 (284.8 eV) can be found, as well as several tail signals in the range of 286–292 eV corresponding to oxygen and nitrogen-containing functional groups [56] (see Supplementary Information Table S1 for details).

Interestingly, the spectrum for CNTs-ox-45 revealed high-intensity signals corresponding to C=N (285.0 eV) and C–N (286.2 eV) (this last also contains a component from C–OH bonds). These signals are also present in the spectra of CNTs-ox-90 and CNTs-ox-180 but are less intense. From here, it can be inferred that nitrogen intercalation in CNTs structure happens at early oxidation stages (45 min). Meanwhile, for longer, the presence of nitrogen might be mostly related to surface functional groups such as –NO$_2$ groups.
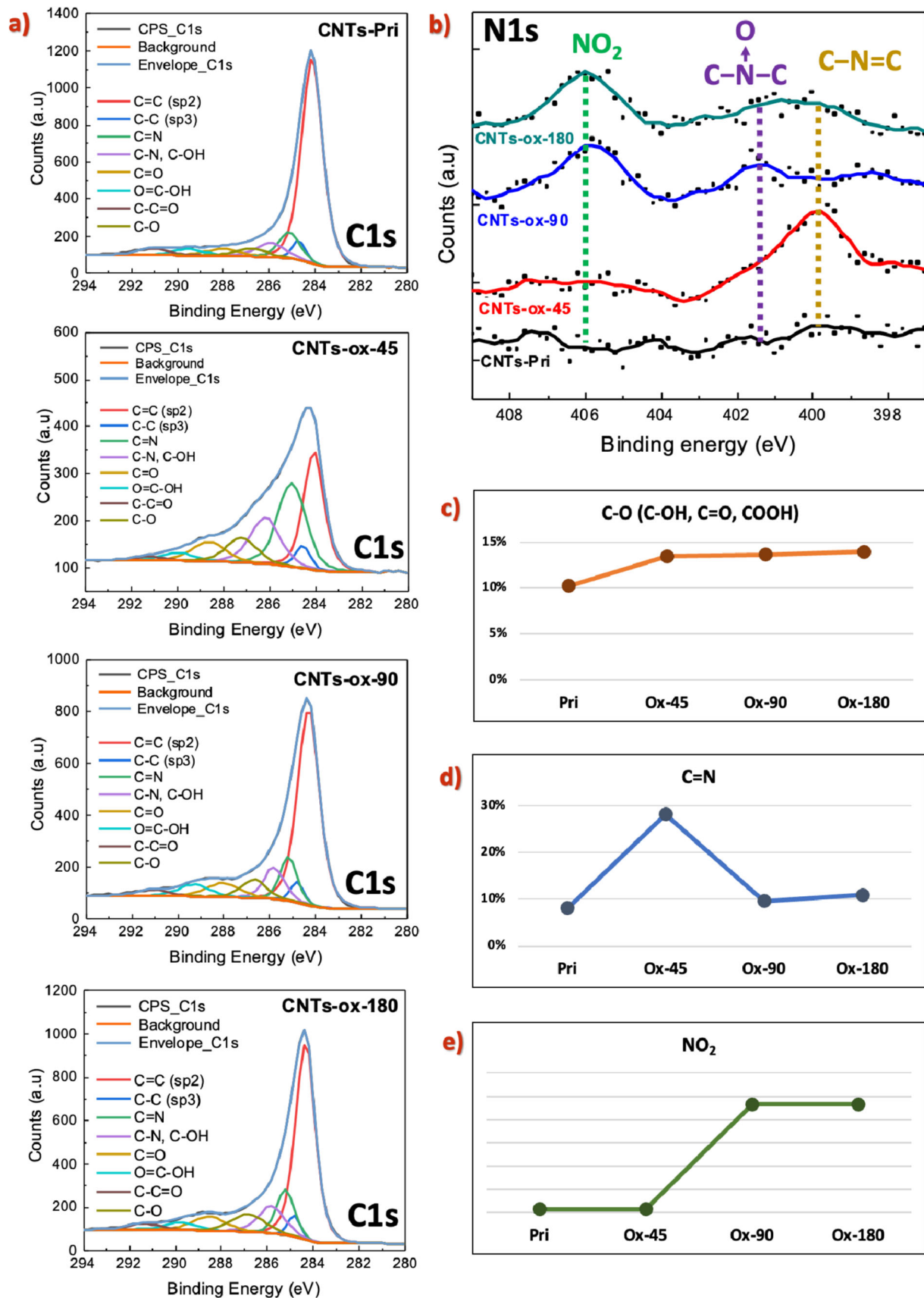
Figure 3 **a** XPS (C1s) spectra for all the CNTs and deconvolution of the signal. **b** XPS (N1s) spectra for the four carbon nanotubes and assignation of peaks. **c** Comparative presence of oxygen-containing functional groups obtained from C1s spectra, **d** nitrogen inserted on CNTs structure (also obtained from C1s spectra), and **e** qualitative comparison of NO_2 functional groups present in the four carbon nanotubes studied (detailed information on these calculations can be found in the Supporting Information, Table S1).

To corroborate this hypothesis, high-resolution N1s XPS spectra were measured in the 399–407 eV range (Fig. 3b). The deconvolution of signals, in this case, can be complex due to the low intensity of the peaks; nevertheless, the smoothed spectra show some revealing findings. As suggested by the C1s spectrum, the CNTs-ox-45 show a peak with a maximum at 399.9 eV, which can be primarily related to C=N–C bonds [57], indicating the presence of nitrogen as a substituent of C atoms in the graphitic structure of CNTs. Then, for 90 min of oxidation, the peak at 399.9 eV is hard to identify; meanwhile, two new signals appear at 401.5 and 406.0 eV (not present for CNTs-Pri nor CNTs-ox-45). The first of these signals can be attributed to N–O bonds formed in the early-stage oxidation of surface nitrogen. In contrast, the signal at 406.0 eV corresponds to NO_2 groups, as previously reported [57, 58]. Finally, the spectrum of CNTs-ox-180 shows mostly a signal at 406.0 eV from NO_2 and a wide band from 403 to 398 eV, probably corresponding to a sum of the previously mentioned signals (C=N–O; C=N–C).

These results suggest that the formation of –NO_2 groups on CNTs surface happens through a multi-step mechanism, where first nitrogen substitutes C atoms in the lattice of CNTs, and later these N atoms are oxidized to form early-stage C–N–O bonds, and finally –NO_2 functional groups.

Finally, Fig. 3c, d shows the quantitative relative percentage of functional groups obtained from the integral of C1s signals (C–O and C=N) peaks and qualitative comparison of –NO_2 presence obtained from the analysis of the peak at 406.0 eV in the N1s spectra. Here, the relative amount of oxygen-containing functional groups and substituent nitrogen both have a maximum for CNTs-ox-45, decreasing for CNTs-ox-90 and then slightly increasing for CNTs-ox-180. This remarkable result proves the complex

nature of CNTs oxidation in nitrating mixtures [55, 59].

As stated by Kolanowska et al., longer oxidation times do not necessarily mean more presence of functional groups. As suggested by these authors, the oxidative mechanism of CNTs undergoes a competitive mechanism between forming functional groups and destroying CNTs walls [59]. Our results indicate that the functionalization is the highest for 45 min of oxidation, while the degradation of CNTs plays an essential role for longer treatment times.

To further analyze and prove this hypothesis, Raman spectroscopy was performed for all CNTs, and the results are presented in Fig. 4. All spectra
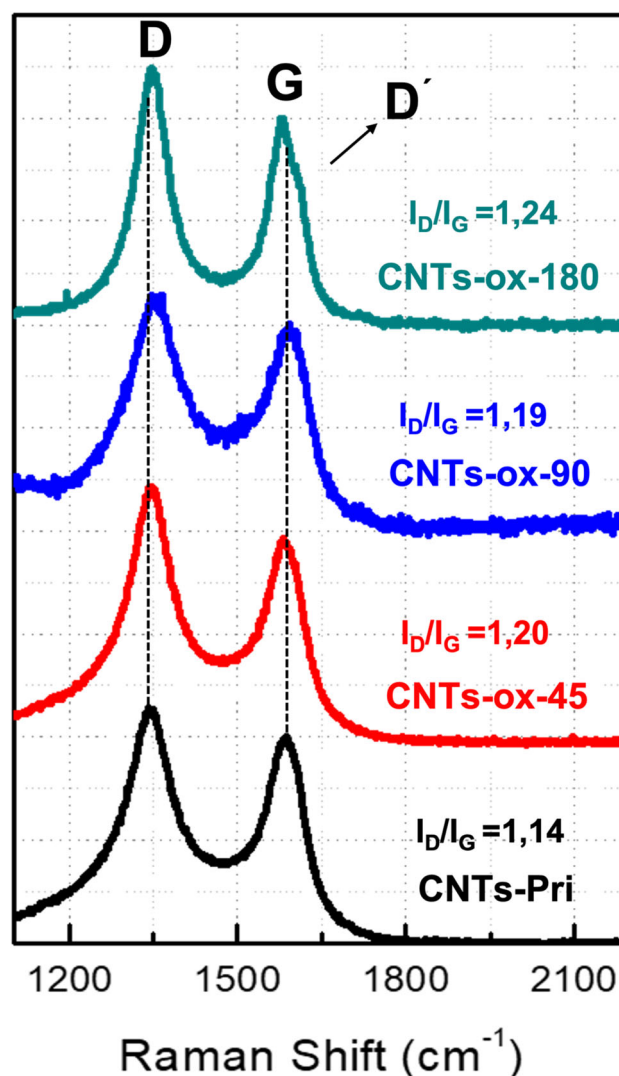

Figure 4 Raman spectra for pristine and oxidized carbon nanotubes, showing the characteristic D and G bands and I_D/I_G ratio.

exhibit the characteristic D and G bands of CNTs, and for the CNTs of maximum oxidation (CNTs-ox-180), a shoulder of the D′ band can be detected [60]. The G band is typical of all graphitic materials. Meanwhile, the D band is generally related to defects (i.e., the presence of sp^3-type carbon in the lattice or surface of CNTs) [61].

The ratio between the D and G band (I_D/I_G) intensities is commonly analyzed to understand the presence of defects in CNTs so that it can be related to the relation between C-sp^3/C-sp^2 [62]. Nevertheless, when amorphous carbon is present, the analysis of I_D/I_G bands should not be the only parameter analyzed, which may lead to contradictions [54, 60]. For a better understanding of the spectra, the interband region between the D and G bands must also be considered, so its intensity can be mostly related to a component of a $5A_1$ vibrational mode (attributed to breathing modes of 5 ring members and indicative of amorphous carbon [54]). Also, the width of D and G bands indicates graphitization, with this parameter being higher when narrower bands are observed [54].

Taking all these parameters into account, an increment in the I_D/I_G ratio from CNTs-Pri to CNTs-ox-45 (from 1.14 to 1.20) can be seen, as well as a decrease in the intensity of the interband region. The introduction of functional groups has been proved to provoke this shift in the I_D/I_G relationship [60], mainly due to the formation of more sp3 bonds (this is supported by XPS analysis of C1s, see Supplementary Information, Table S1). Also, the decrease in the intensity of the interband region can be associated with the elimination of amorphous carbon present in CNTs-Pri (remaining from the CVD synthetic procedure and not completely removed in the purification process).

On the other hand, from CNTs-ox-45 to CNTs-ox-90, the I_D/I_G ratio decreases slightly (from 1.20 to 1.19). Also, the interband region shows a higher intensity. As suggested by the XPS analysis, in this case, the presence of sp3 atoms is less, and some amorphous carbon is formed. This is congruent with the hypothesis that longer oxidation times lead to CNTs degradation.

Finally, when increasing the oxidation time to 180 min, the ID/IG ratio is increased from 1.2 to 1.24 due to a more significant presence of functional groups. Also, for CNTs-ox-180, a shoulder corresponding to the D′ band indicates more disorders [63]. Additionally, the Raman spectrum of this sample (green line in Fig. 4) shows a decrease in both G and D line widths. This, along with the reduction of intensity in the interband region, suggests that a long oxidation time leads to the degradation of CNTs (elimination of amorphous carbon and exposure of the inner walls). Previous studies have found that prolonged oxidative treatments lead to the digestion of CNTs, which may explain the observed result [62].

TEM images were also obtained to further analyze the effect of the oxidative treatment on CNTs structure (Fig. 5a). As expected from Raman spectroscopy analysis, the increase in oxidation time provokes the degradation of CNTs, leading to rougher and grooves-containing walls. For CNTs-ox-45, the degradation of walls cannot be seen from this TEM analysis. Meanwhile, degradation is more evident for CNTs-ox-90, and the results show that the CNTs-ox-180 are the most damaged, as previously stated when analyzing the Raman spectra.

The previously stated hypothesis can be verified by examining the wall width of CNTs (Fig. 5b). As the oxidation time increases, the overall width of CNTs decreases from 26 ± 7 nm in CNTs-Pri to 19 ± 4 nm (CNTs-ox-45), 16 ± 3 nm (CNTs-ox-90), and 12 ± 3 nm (CNTs-ox-180). These results are similar to those obtained by Kolanowska et al., where the oxidation of carbon nanotubes was studied as a function of time using a nitrating mixture (HNO_3/H_2SO_4 1/3 (v/v)) [62]. There it was proven that the treatment consists of two competitive processes: functionalization of CNTs and external wall degradation, which is similar to our findings in this work.

In summary, the duration of CNTs oxidation in HNO_3/H_2SO_4 induces different extents of CNTs functionalization, defect presence, and sidewall degradation: 45 min of oxidation leads to CNTs with the highest amount of oxygen functional groups, as well as the presence of nitrogen as a substituent in the structure. Also, amorphous carbon is removed to some extent, and the external wall width decreases. Increasing the oxidation time from 45 to 90 min favors the formation of nitro groups on the CNTs' surface. At the same time, the extent of degradation of CNTs walls is more significant compared to 45 min. Finally, doubling the oxidation time from 90 to 180 min again provokes the destruction of CNTs' external walls despite introducing many new functional groups.

These characteristics are genuinely relevant for CNTs-TiO_2 interactions and charge transfer in the

Figure 5 **a** TEM images of pristine and oxidized CNTs, and **b** CNTs width distribution obtained from TEM images analysis (Mean sizes ± SD are shown).
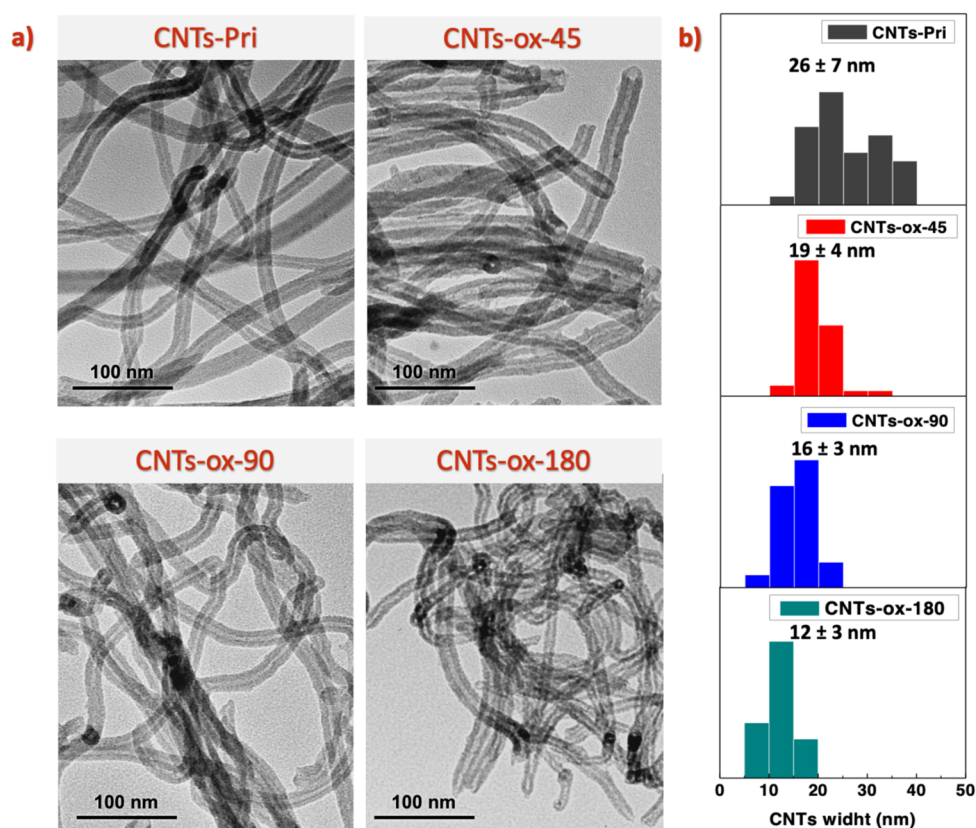
composites: the noteworthy presence of functional groups (especially chelating groups such as $-NO_2$ and $-COOH$) may lead to a better interaction between both materials. At the same time, CNTs with a high level of wall destruction and loss of symmetry may lead to poor interactions with the semiconductor and act as recombination sites, affecting the photoelectrochemical performance.

ITO/CNTs-ox/TiO$_2$ thin film photoelectrodes

Structural and morphological properties

Significant differences occurred when TiO_2 was grown over the CNTs-Pri and the three oxidized CNTs (previously deposited on ITO). Figure 6 shows optical images of the four photoelectrodes prepared and Raman spectra of different zones of the films: CNTs agglomerates (bulky CNTs zones) and disperse zones (where CNTs agglomerates are not observed).

The optical images show a clear difference in dispersion in comparison between CNTs-Pri, CNTs-ox-45, CNTs-ox-90, and CNTs-ox-180. For CNTs-Pri, mostly large agglomerates are found, corresponding to their poor propanol dispersion before being drop-casted on ITO substrates (See Supplementary Information, Figure S2). For CNTs-ox-45, the presence of agglomerates is also relevant, and in the case of CNTs-ox-180, most of the CNTs are forming large-size agglomerates. However, in the case of CNTs-ox-90, better dispersion of CNTs is observed, leading to small agglomerates and the homogeneous presence of CNTs over the film.

This can be understood because of two phenomena: the dispersion of CNTs before being drop-casted and the interaction between CNTs when the solvent evaporates from the ITO surface. Regarding CNTs dispersion in 2-propanol, the oxidation of CNTs leads to the presence of functional groups, which allows for enhanced interaction with the solvent. This justifies the better dispersion observed for all CNTs-ox in comparison with CNTs-Pri.

Nevertheless, when drop-casted on the ITO surface, the interaction between neighboring nanotubes plays a relevant role. CNTs-Pri are weakly dispersed, so the formation of agglomerates is evident (Fig. 6a). For CNTs-ox-45 (Fig. 6b), the presence of oxygen functional groups is higher (Fig. 3c), as well as the
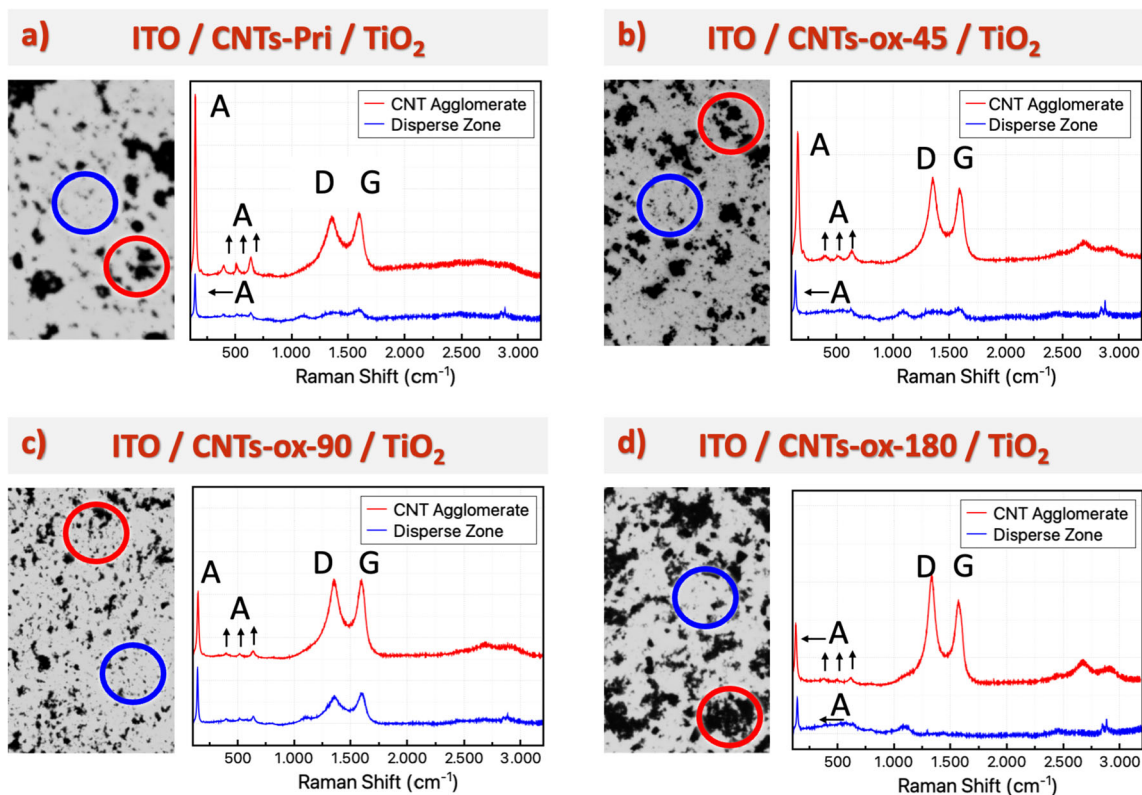
Figure 6 Optical images (left) and micro-Raman spectra (right) of disperse zones (blue) and zones where CNTs agglomerate (red) on the surface of all films prepared: **a** ITO/CNTs-Pri/TiO$_2$, **b** ITO/CNTs-ox-45-TiO$_2$ **c** ITO/CNTs-ox-90-TiO$_2$ and **d** ITO/CNTs-ox-180-TiO$_2$).

presence of sp3 carbon (Supporting Information, Table 1). Despite functional groups allowing a good dispersion of CNTs in propanol, a considerable presence of these groups combined with a high number of defective sp3 surface carbon atoms may also favor the interaction of neighboring CNTs through dipole–dipole interactions leading to agglomeration.

For CNTs-ox-90, the degradation of walls starts to play a competitive role with CNTs functionalization, and the presence of sp3 carbons is less than for CNTs-ox-45, as analyzed in Sect. "CNTs: functionalization and Structure". As a result, these CNTs show a better long-term dispersion (Supplementary Information Figure S2) than CNTs-ox-45, which may probably result from fewer sp3 defective carbons and oxygenated groups (and, as a result, fewer interactions between CNTs). As a result, when drop-cast on the ITO surface, the Brownian motion of CNTs does not lead to agglomeration, and a more homogeneous layer of CNTs is obtained (Fig. 6c).

On the other hand, CNTs surface destruction in CNTs-ox-180 provokes the exposure of the inner

walls of CNTs despite favoring the formation of new functional groups. As a result, π–π and Van-der Waals interactions between neighboring CNTs are favored, provoking poor dispersion of these CNTs in propanol (Supplementary Information Figure S2) and the formation of agglomerates when drop-casted on the ITO surface (Fig. 6d).

The homogeneous dispersion of CNTs on the surface of ITO is crucial for TiO$_2$ growth. Raman spectra of all films show that TiO$_2$ favorably grows over CNTs structures, which can be corroborated by the simultaneous presence of the four anatase signals at 153, 396, 510, and 633 cm^{-1} and CNTs' D and G bands at 1350 and 1597 cm^{-1}, respectively. The precise frequencies of these bands for every sample are summarized in Table S2 (Supporting Information). In all cases, these signals are observed when analyzing Raman spectra of the CNTs agglomerates (red lines in Fig. 6). Interestingly, when Raman spectra are measured in disperse areas, in CNTs-Pri/TiO$_2$ and both CNTs-ox-45/TiO$_2$ and CNTs-ox-180/TiO$_2$ samples, only the most intense anatase signal (144) can be found, combined with the poor presence of CNTs'

bands. However, in the CNTs-ox-90/TiO$_2$ samples, CNTs are also present in the disperse zones. The four Raman signals of anatase are seen, indicating the formation of a homogeneous TiO$_2$-CNTs structure over the entire substrate.

The presence of the anatase phase in all CNTs/ TiO$_2$ films was confirmed using XRD. The most intense peak of anatase at 25.4° corresponding to (101) planes could be identified in all films, and also, a peak at 48.4° related to (200) planes is generally observed [64] (Supplementary Information, Figure S3).

SEM images of the four films were analyzed to study their morphology (Fig. 7). In low-magnification images, a CNTs network can be observed deposited on the surface and covered by a TiO$_2$ layer. Nevertheless, there are significant differences in the characteristics of the TiO$_2$ structures formed depending on the oxidation degree of the CNTs employed as substrates. A better appreciation can be made by
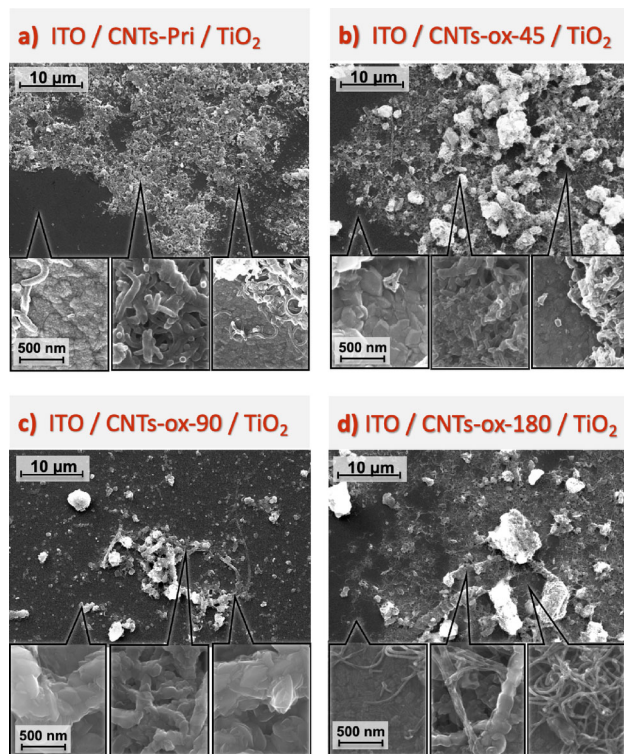
evaluating high-magnification images (insets in Fig. 7).

Three main sites were examined for every sample: zones where no CNTs are observed (disperse zones), CNTs agglomerates, and zones surrounding areas of CNTs agglomerates. The agglomeration of CNTs on the surface undoubtedly defined how titanium dioxide grows over the substrate. Samples with a high presence of CNT agglomerates (i.e., CNTs-Pri/ TiO$_2$, CNTs-ox-45/TiO$_2$, and CNTs-ox-180/TiO$_2$) show a high heterogeneity regarding TiO$_2$ growth, meanwhile, for CNTs-ox-90/TiO$_2$ the presence of well-dispersed CNTs allowed the formation of a more robust and homogenous TiO$_2$ layer.

The transversal views of the films are shown in Fig. 8. These corroborated the presence of big CNTs-agglomerates in the case of CNTs-Pri, CNTs-ox-45, and CNTs-ox-180; meanwhile, only for CNTs-ox-90 a homogeneous thin CNTs-TiO$_2$ layer of about 550–600 nm was formed.

Also, the quality of TiO$_2$ crystals found in CNTs-ox/TiO$_2$ samples is higher than for the untreated nanotubes, and the crystal sizes are larger. As was stated in Sect. "CNTs: functionalization and structure", CNTs-ox have a superior population of surface functional groups that serve as TiO$_2$ nucleation sites, favoring the formation of a more compact and cohesive structure. Then, the oxidation of CNTs plays a crucial role in the physical dispersion of CNTs and the chemical interaction with this semiconductor material. This result has also been reported for similar composites [24, 38, 65, 66].
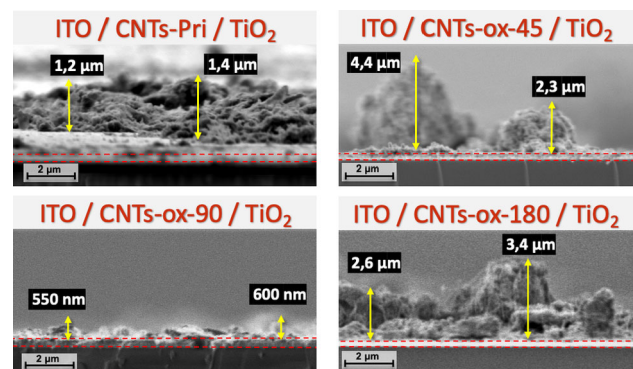

Figure 7 SEM images for all the CNTs-/TiO$_2$ films prepared. Insets show magnification of TiO$_2$ structures grown over the ITO/ CNTs surface. **a** ITO/CNTs-Pri/TiO$_2$; **b** ITO/CNTs-ox-45/TiO$_2$; **c** ITO/CNTs-ox-90/TiO$_2$; and **d** ITO/CNTs-ox-180/TiO$_2$). This figure also presents detailed high-resolution images in Supporting Information, Figure S4.

Figure 8 Transversal SEM images for the studied four ITO/ CNTs/TiO$_2$ electrodes.

Optical properties

The optical properties of ITO/CNTs-X/TiO$_2$ were studied through UV–Vis diffuse reflectance spectroscopy (Fig. 9a). To determine bandgaps, these spectra were transformed using the Kubelka–Munk function $(\alpha h\upsilon)^{1/2}$ as a function of photon energy ($h\upsilon$). Here α corresponds to the absorption coefficient (Supplementary Information, Figure S5).

In all cases, a steep linear increment of light absorption is observed with increasing energy, typical of semiconductor materials [67]. The bandgap values were determined from a linear fit of this linear region using the Tauc equation and are presented in Fig. 9b (square symbols).

As noted in all the transformed diffuse reflectance graphs, there is an additional absorption region at energies below the bandgap value (Figure S5). This
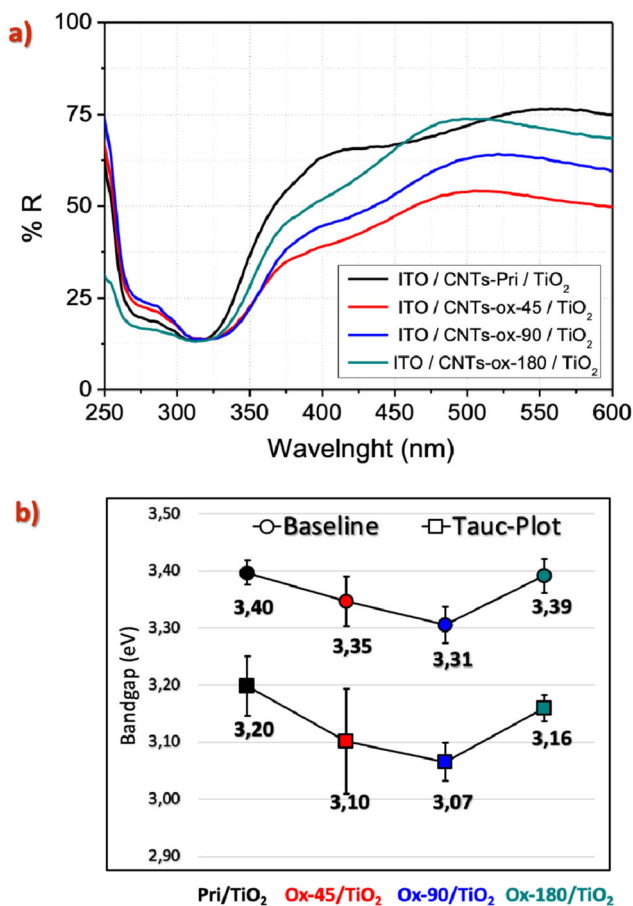

phenomenon is characteristic of composites, where the optical properties of the other materials may lead to additional absorption at energies below the TiO$_2$ bandgap. In these cases, a straightforward interpretation of the Tauc plots may lead to a misinterpretation of the bandgap value. Makuła et al. developed a simple method to obtain more accurate bandgap values in these cases, constructing a baseline by making a linear fit of the slope below the fundamental absorption [67]. Then the bandgap value corresponds to this line's intercept and the main absorption's linear fit. The bandgap values determined by this method are also shown in Fig. 9b (circles).

Bandgap values determined by the Baseline method are all higher than those determined employing a simple Tauc Plot, as was previously reported by Makuła et al. [67]. Nevertheless, the tendency in bandgap values is the same in both cases. CNTs-Pri-TiO$_2$ show the higher value, while somewhat smaller values are obtained when using oxidized CNTs, being the smallest for CNTs-ox-90. Meanwhile, for CNTs-ox-180, the bandgap increases again, being similar to the value obtained for untreated CNTs.

These results can be understood as a consequence of CNTs-TiO$_2$ interaction and the bonding strength between both structures. It has been proved that CNTs enhance surface electrical charge in TiO$_2$ nanomaterials leading to a redshift in the bandgap value [38]. Therefore, stronger interactions between both materials lead to more significant displacement. This is relevant for photoelectrochemical applications; hence, a smaller bandgap would improve light absorption in the visible region.

In this sense, the results correspond with the materials' morphological structure (see Sect. "optical properties"). CNTs-Pri proved to have a weak interaction with TiO$_2$, leading to poor growth of TiO$_2$ on their surface. Meanwhile, introducing functional groups on their surface (CNTs-ox-45 and CNTs-ox-90) leads to an improved cohesion with TiO$_2$, favored by polar groups such as –COOH, –OH, and –NO$_2$. An optimal interaction is obtained for CNTs-ox-90, where the material appeared most homogeneous with larger crystal sizes. Meanwhile, the increment in agglomeration observed for CNTs-ox-180 leads to a weaker interaction with TiO$_2$, reflected in the higher bandgap value observed compared to CNTs with an intermediate oxidation extent.

Figure 9 a Diffuse reflectance spectra for all ITO/CNTs/TiO$_2$ samples. **b** Determined bandgap values by using the baseline method (circles) [67] and Tauc plots (squares) for a set of ITO/CNTs/TiO$_2$ samples, with nine replicates each. Standard error bars are shown in every case (see Table S3 for details).

Photoelectrochemical properties

The electrodes were evaluated in a three-electrode cell to evaluate further the effect of the morphological and optical properties of the films on their photoelectrochemical response. Figure 10a presents linear sweep voltammetry curves in the dark and under illumination (100 mW/cm^2, Xenon arc-lamp). In all cases, the dark current is negligible. Under illumination, the electrodes show a typical n-type semiconductor material behavior: a steep rise in photocurrent appears between -0.4 and 0 V, and then a photocurrent plateau appears, with a smooth surge in photocurrent for higher applied potential values. CNTs-ox-90/TiO$_2$ shows the best photoelectrochemical response as the steep linear rise in photocurrent is achieved at a lower potential, and the photocurrent value at the plateau is higher. The photocurrent in this inert electrolyte solution corresponds to water oxidation, a determining process for solar water-splitting systems.

The inset shows the normalized photocurrent values for four samples at 0.5 V vs. Ag/AgCl. Here, a dependence on the response as a consequence of the degree of oxidation of the nanotubes can also be found. Oxidized CNTs (45 and 90) show a better response than CNTs-Pri, with the best performance for CNTs-ox-90, while for CNTs-ox-180, the photoresponse diminishes the same as that for untreated CNTs.

This result is a combination of the effects previously analyzed. A better photoresponse is obtained for the material with a more homogenous TiO$_2$ layer and smaller bandgap value. The better interaction between CNTs and the semiconductor led to enhanced charge transfer and decreased bandgap energy (as described in Sect. "Optical properties"). Also, the absence of bulky agglomerates may allow for better conduction of photogenerated electrons to the ITO collector. Improved transport would also lead to reduced recombination as charge extraction is faster.

Photoelectrodes were also studied using transient chronoamperometry scans (Fig. 10b). The same tendency was seen, supporting the previous analysis. Interestingly, when the light is switched on in all the samples containing oxidized CNTs, there is a rapid increase in current density, followed by a drop to steady-state value under illumination. This behavior has been previously noted on similar materials fabricated by us, in that case on silicon wafers [52] and in other reports where carbon materials are combined with TiO$_2$. In this case, fast charge separation is achieved when illuminating, followed by a drop to steady-state due to recombination. The difference between oxidized and untreated carbon nanotubes may be related to the presence of surface defects that function as recombination sites.

Conclusion and perspective

The results show that the oxidation of carbon nanotubes in a nitrating mixture (9/10) consists of a competitive functionalization mechanism and external wall degradation. This competitive mechanism between functionalization and CNTs degradation proved very relevant regarding the fabrication of CNTs-TiO$_2$ photoelectrodes.

The oxidation of CNTs is crucial to achieving adequate dispersion and enhancing the interaction with TiO$_2$. The dispersibility of CNTs plays a particularly crucial role in attaining homogeneous TiO$_2$ deposits, which show significantly improved photoelectrochemical properties.

For the shortest oxidation time studied (45 min), the major oxidation was found (proved by the high presence of oxygenated groups and sp3 carbon). Nevertheless, a more significant oxidation degree did not translate into a better dispersion in propanol or a more homogeneous film on the ITO surface by drop-casting. Instead, a high presence of sp3 carbon and oxygenated groups provoked CNTs agglomeration. The growth of TiO$_2$ over these CNTs was improved in comparison with CNTs-Pri, due to the presence of functional groups acting as nucleation sites. However, the presence of CNT agglomerates disfavored the formation of a homogeneous TiO$_2$ layer.

For the material obtained after 90 min. of oxidation, the presence of oxygenated functional groups was lower, and NO$_2$ groups were formed due to the oxidation of nitrogen dopants introduced in CNTs in the first steps of the oxidation mechanisms. As a result, these CNTs showed better dispersion, forming a homogeneous deposit on ITO after drop casting. The homogeneity of the ITO/CNTs-ox-90 substrate allowed for the growth of a regular TiO$_2$ layer, with enhanced cohesion with CNTs, and thereupon the obtained ITO/CNTs-ox-90/TiO$_2$ photoelectrode showed an improved performance.

Figure 10 **a** Typical linear sweep voltammetry curves in the dark and under illumination for all samples. The inset summarizes the normalized values of photocurrent obtained for five samples (at 0.5 V vs. Ag/AgCl; standard error bars are shown in every case). **b** Chronoamperometry scans under chopped light at 0.5 V vs. Ag/AgCl.
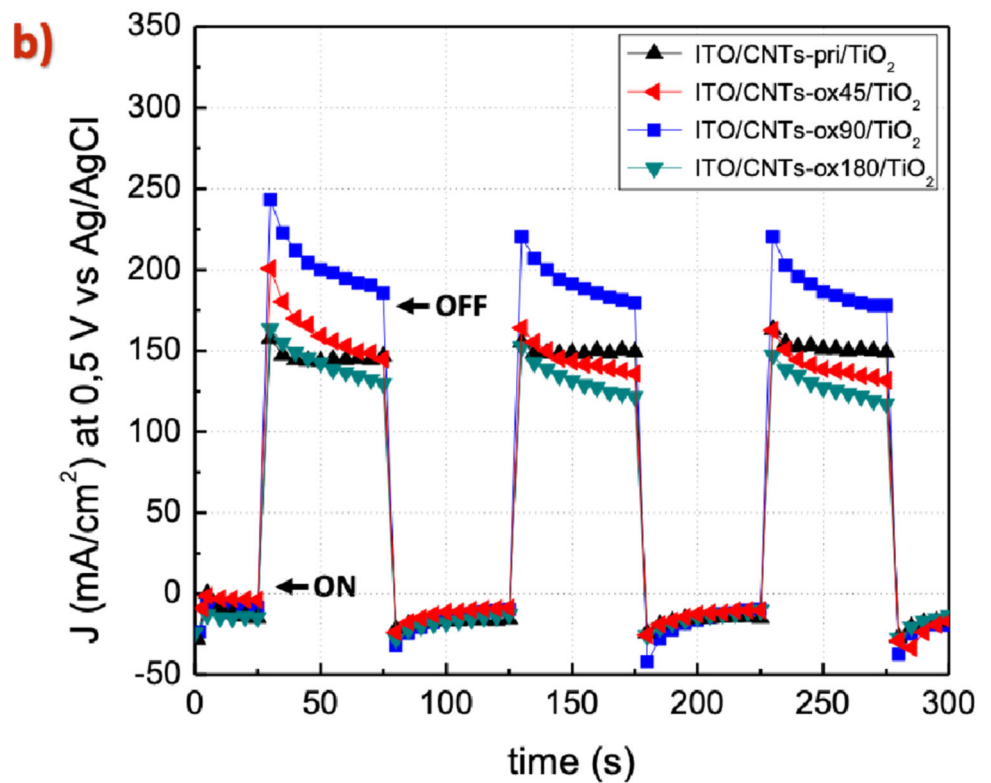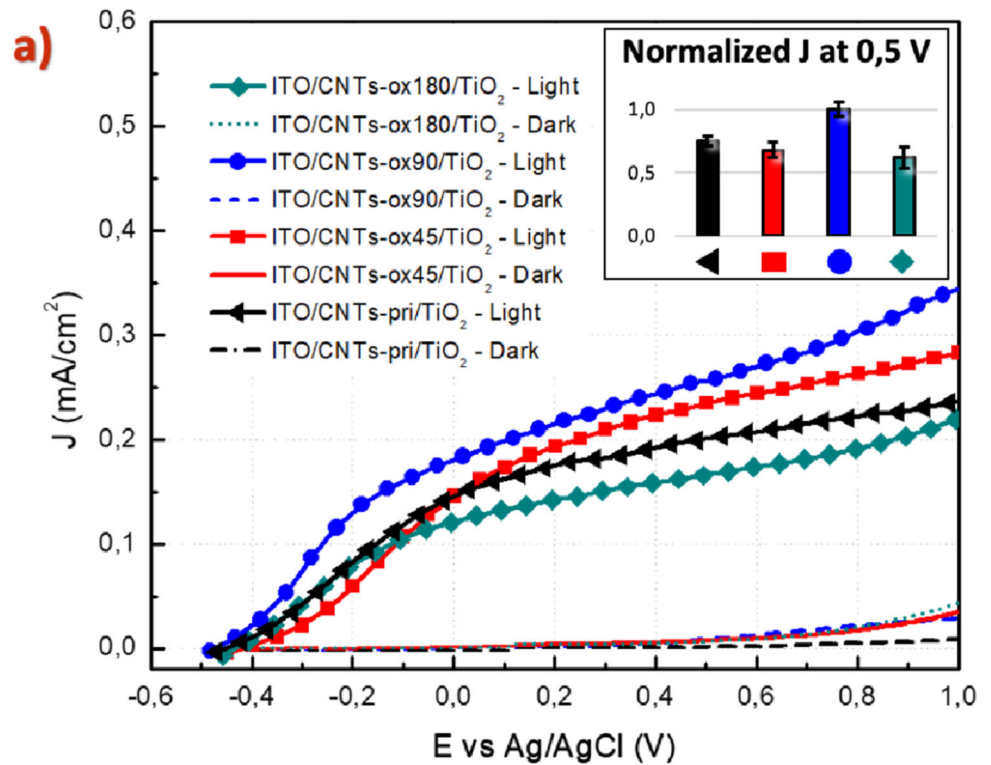
Finally, after introducing new functional groups, 180 min of treatment severely damaged CNTs, leading to external wall degradation. As a result, this material showed poor dispersion, the formation of bulky agglomerates, and poor interaction with TiO$_2$ leading to a photoelectrode of poor performance.

In conclusion, analyzing only the functionalization of CNTs for the composites fabrication may lead to erroneous assumptions since a more prominent presence of functional groups does not necessarily mean a better formation of CNTs-TiO$_2$ composites. Consequently, it is essential to understand the effect of oxidation in all the properties of CNTs (i.e., functional groups presence, surface defects, thickness) and how this may be related to other properties of composites. Further works are encouraged to consider the broad phenomena to achieve CNTs-semiconductors composites with optimized performance.

On the other hand, further research is necessary to deeply understand the role of oxidized carbon in the photoelectrochemical performance of TiO$_2$ anodes or other semiconductor materials with better performance. Although these composites are interesting for studies like the one conducted in this research, TiO$_2$ has significant limitations regarding visible light absorption. In this sense, the combination of CNTs-ox-TiO$_2$ photoelectrodes to other materials (such as quantum dots, plasmonic nanoparticles, or the fabrication of Tandem devices) is a very promising field of research.

Declarations

Conflict of interest The authors declare that they have no known competing financial interests or personal relationships that could have appeared to influence the work reported in this paper.

Ethical approval This study does not involve experiments with human tissue or others requiring bioethical approval.

Supplementary Information: The online version contains supplementary material available at https://doi.org/10.1007/s10853-023-08351-4.

References

[1] Hosseini SE, Wahid MA (2020) Hydrogen from solar energy, a clean energy carrier from a sustainable energy source. Int J Energy Res 44:4110–4131. https://doi.org/10.1002/er.4930

[2] McFarland E (2022) Photoelectrochemical hydrogen generation. Springer Nature Singapore, Singapore

[3] Yang W, Prabhakar RR, Tan J et al (2019) Strategies for enhancing the photocurrent, photovoltage, and stability of photoelectrodes for photoelectrochemical water splitting. Chem Soc Rev 48:4979–5015. https://doi.org/10.1039/C8CS00997J

[4] Tang S, Qiu W, Xiao S et al (2020) Harnessing hierarchical architectures to trap light for efficient photoelectrochemical cells. Energy Environ Sci 13:660–684. https://doi.org/10.1039/c9ee02986a

[5] Ding X, Gao Y, Zhang L et al (2014) Visible light-driven water splitting in photoelectrochemical cells with supramolecular catalysts on photoanodes. ACS Catal 4:2347–2350. https://doi.org/10.1021/CS500518K/SUPPL_FILE/CS500518K_SI_001.PDF

[6] Youngblood JW, Lee SHA, Kobayashi Y et al (2009) Photoassisted overall water splitting in a visible light-absorbing dye-sensitized photoelectrochemical cell. J Am Chem Soc 131:926–927. https://doi.org/10.1021/JA809108Y/SUPPL_FILE/JA809108Y_SI_001.PDF

[7] Zhao Y, Swierk JR, Megiatto JD et al (2012) Improving the efficiency of water splitting in dye-sensitized solar cells by using a biomimetic electron transfer mediator. Proc Natl Acad Sci USA 109:15612–15616. https://doi.org/10.1073/PNAS.1118339109/ASSET/D54F58A7-3F74-48B2-9A30-5

23CF13B9DE4/ASSETS/GRAPHIC/PNAS.1118339109E Q6.GIF

[8] Liao F, Shi Y, Dang Q et al (2022) Carbon dots dominated photoelectric surface in titanium dioxide nanotube/nitrogen-doped carbon dot/gold nanocomposites for improved photoelectrochemical water splitting. J Colloid Interface Sci 606:1274–1283. https://doi.org/10.1016/J.JCIS.2021.08.131

[9] Li S, Liu C, Chen P et al (2020) In-situ stabilizing surface oxygen vacancies of TiO_2 nanowire array photoelectrode by N-doped carbon dots for enhanced photoelectrocatalytic activities under visible light. J Catal 382:212–227. https://doi.org/10.1016/j.jcat.2019.12.030

[10] Luo H, Dimitrov S, Daboczi M et al (2020) Nitrogen-doped carbon dots/TiO_2 nanoparticle composites for photoelectrochemical water oxidation. ACS Appl Nano Mater 3:3371–3381. https://doi.org/10.1021/acsanm.9b02412

[11] Wang H, Bai Y, Zhang H et al (2010) CdS quantum dots-sensitized TiO_2 nanorod array on transparent conductive glass photoelectrodes. J Phys Chem C 114:16451–16455. https://doi.org/10.1021/jp104208z

[12] Selopal GS, Mohammadnezhad M, Besteiro LV et al (2020) Synergistic effect of plasmonic gold nanoparticles decorated carbon nanotubes in quantum dots/TiO_2 for optoelectronic devices. Adv Sci. https://doi.org/10.1002/advs.202001864

[13] Sahai S, Ikram A, Rai S et al (2017) Quantum dots sensitization for photoelectrochemical generation of hydrogen: a review. Renew Sustain Energy Rev 68:19–27. https://doi.org/10.1016/j.rser.2016.09.134

[14] Zhou T, Chen S, Li L et al (2020) Carbon quantum dots modified anatase/rutile TiO_2 photoanode with dramatically enhanced photoelectrochemical performance. Appl Catal B. https://doi.org/10.1016/J.APCATB.2020.118776

[15] Tao J, Sun Z, Cheng Y et al (2017) Enhanced photoelectrochemical properties of nanocrystalline TiO_2 electrode by surface sensitization with CuxO quantum dots. Sci Rep 7:5291. https://doi.org/10.1038/s41598-017-05645-x

[16] Díaz FJP, del Río RS, Rodriguez PEDS (2022) Plasmonic photocatalysts for water splitting, pp 117–173

[17] Warren SC, Thimsen E (2012) Plasmonic solar water splitting. Energy Environ Sci 5:5133–5146. https://doi.org/10.1039/c1ee02875h

[18] Lee J, Mubeen S, Ji X et al (2012) Plasmonic photoanodes for solar water splitting with visible light. Nano Lett 12:5014–5019. https://doi.org/10.1021/nl302796f

[19] Gellé A, Moores A (2017) Water splitting catalyzed by titanium dioxide decorated with plasmonic nanoparticles. Pure Appl Chem 89:1817–1827. https://doi.org/10.1515/pac-2017-0711

[20] Valenti M, Jonsson MP, Biskos G et al (2016) Plasmonic nanoparticle-semiconductor composites for efficient solar water splitting. J Mater Chem A Mater 4:17891–17912. https://doi.org/10.1039/c6ta06405a

[21] Zhang X, Wang X, Yi X et al (2020) Metal-reduced WO 3–x electrodes with tunable plasmonic resonance for enhanced photoelectrochemical water splitting. ACS Appl Energy Mater 3:3569–3576. https://doi.org/10.1021/acsaem.0c00086

[22] Zhang Z, Zhang L, Hedhili MN et al (2013) Plasmonic gold nanocrystals coupled with photonic crystal seamlessly on TiO_2 nanotube photoelectrodes for efficient visible light photoelectrochemical water splitting. Nano Lett 13:14–20. https://doi.org/10.1021/nl3029202

[23] Ghobadi TGU, Ghobadi A, Soydan MC et al (2020) Strong light-matter interactions in Au plasmonic nanoantennas coupled with Prussian blue catalyst on $BiVO_4$ for photoelectrochemical water splitting. Chemsuschem 13:2577–2588. https://doi.org/10.1002/cssc.202000294

[24] Rai S, Ikram A, Sahai S et al (2017) CNT based photoelectrodes for PEC generation of hydrogen: a review. Int J Hydrog Energy 42:3994–4006. https://doi.org/10.1016/j.ijhydene.2016.10.024

[25] Reza MS, Ahmad NBH, Afroze S et al (2022) Hydrogen production from water splitting through photocatalytic activity of carbon-based materials. Chem Eng Technol

[26] Jumeri FA, Lim HN, Zainal Z et al (2014) Titanium dioxide-reduced graphene oxide thin film for photoelectrochemical water splitting. Ceram Int 40:15159–15165. https://doi.org/10.1016/j.ceramint.2014.06.130

[27] Wang B, Sun Q, Liu S, Li Y (2013) Synergetic catalysis of CuO and graphene additives on TiO_2 for photocatalytic water splitting. Int J Hydrog Energy 38:7232–7240. https://doi.org/10.1016/j.ijhydene.2013.04.038

[28] Bellamkonda S, Thangavel N, Hafeez HY et al (2019) Highly active and stable multi-walled carbon nanotubes-graphene-TiO_2 nanohybrid: an efficient non-noble metal photocatalyst for water splitting. Catal Today 321–322:120–127. https://doi.org/10.1016/j.cattod.2017.10.023

[29] Esmaili H, Kowsari E, Ramakrishna S et al (2022) Sensitization of TiO_2 nanoarrays by a novel palladium decorated naphthalene diimide functionalized graphene nanoribbons for enhanced photoelectrochemical water splitting. Mater Today Chem 24:100900. https://doi.org/10.1016/J.MTCHEM.2022.100900

[30] Ullah F, Bashiri R, Muti Mohamed N et al (2022) Exploring graphene quantum dots@TiO_2 rutile (0 1 1) interface for visible-driven hydrogen production in photoelectrochemical cell: density functional theory and experimental study. Appl Surf Sci 576:151871. https://doi.org/10.1016/J.APSUSC.2021.151871

[31] Zhou S, Liu S, Su K, Jia K (2020) Graphite carbon nitride coupled S-doped hydrogenated TiO_2 nanotube arrays with improved photoelectrochemical performance. J Electroanal Chem 862:114008. https://doi.org/10.1016/j.jelechem.2020.114008

[32] Su J, Zhu L, Chen G (2016) Ultrasmall graphitic carbon nitride quantum dots decorated self-organized TiO_2 nanotube arrays with highly efficient photoelectrochemical activity. Appl Catal B 186:127–135. https://doi.org/10.1016/j.apcatb.2015.12.050

[33] Fan X, Wang T, Gao B et al (2016) Preparation of the TiO_2/graphic carbon nitride core-shell array as a photoanode for efficient photoelectrochemical water splitting. Langmuir 32:13322–13332. https://doi.org/10.1021/acs.langmuir.6b03107

[34] Su J, Zhu L, Geng P, Chen G (2016) Self-assembly graphitic carbon nitride quantum dots anchored on TiO_2 nanotube arrays: an efficient heterojunction for pollutants degradation under solar light. J Hazard Mater 316:159–168. https://doi.org/10.1016/j.jhazmat.2016.05.004

[35] Patil SS, Johar MA, Hassan MA et al (2018) Anchoring MWCNTs to 3D honeycomb ZnO/GaN heterostructures to enhancing photoelectrochemical water oxidation. Appl Catal B 237:791–801. https://doi.org/10.1016/j.apcatb.2018.06.047

[36] Ahmed AM, Mohamed F, Ashraf AM et al (2020) Enhanced photoelectrochemical water splitting activity of carbon nanotubes@TiO_2 nanoribbons in different electrolytes. Chemosphere 238:124554. https://doi.org/10.1016/j.chemosphere.2019.124554

[37] Prasadam VP, Flores AMH, Audinot JN, Bahlawane N (2022) CNT-ZnO core-shell photoanodes for photoelectrochemical water splitting. Coatings 12:47. https://doi.org/10.3390/COATINGS12010047/S1

[38] Delekar SD, Dhodamani AG, More KV et al (2018) Structural and optical properties of nanocrystalline TiO_2 with multiwalled carbon nanotubes and its photovoltaic studies using Ru(II) sensitizers. ACS Omega 3:2743–2756. https://doi.org/10.1021/acsomega.7b01316

[39] Mohammadnezhad M, Selopal GS, Wang ZM et al (2020) Role of carbon nanotubes to enhance the long-term stability of dye-sensitized solar cells. ACS Photonics 7:653–664. https://doi.org/10.1021/acsphotonics.9b01431

[40] Yang J, Ganesan P, Ishihara A, Nakashima N (2019) Carbon nanotube-based non-precious metal electrode catalysts for fuel cells, water splitting and zinc-air batteries. ChemCatChem 11:5929–5944. https://doi.org/10.1002/cctc.201901785

[41] Chen P, Wang L, Wang P et al (2015) CNT-$TiO_2$$-\delta$ composites for improved co-catalyst dispersion and stabilized photocatalytic hydrogen production. Catalysts 5:270–285. https://doi.org/10.3390/CATAL5010270

[42] Zolfaghari-Isavandi Z, Shariatinia Z (2018) Fabrication of CdS quantum dot sensitized solar cells using nitrogen functionalized CNTs/TiO_2 nanocomposites. Diam Relat Mater 81:1–15. https://doi.org/10.1016/j.diamond.2017.11.004

[43] Suwazono Y, Murayoshi T, Nagai H, Sato M (2021) Facile fabrication of single-walled carbon nanotube/anatase composite thin film on quartz glass substrate for translucent conductive photoelectrode. Nanomaterials. https://doi.org/10.3390/nano11123352

[44] Le AQH, Nguyen NNT, Tran HD et al (2022) A TiO_2@-MWCNTs nanocomposite photoanode for solar-driven water splitting. Beilstein J Nanotechnol 13:1520–1530. https://doi.org/10.3762/bjnano.13.125

[45] Campos Guaglianoni W, Garcia AP, Basegio TM et al (2021) Influence of CVD parameters on Co-TiO_2/CNT properties: a route to enhance energy harvesting from sunlight. Int J Appl Ceram Technol 18:1297–1306. https://doi.org/10.1111/ijac.13773

[46] Olivares F, Peón F, Henríquez R, del Río RS (2022) Strategies for area-selective deposition of metal nanoparticles on carbon nanotubes and their applications: a review. J Mater Sci 57:2362–2387. https://doi.org/10.1007/s10853-021-06710-7

[47] Cañete-Rosales P, Ortega V, Álvarez-Lueje A et al (2012) Influence of size and oxidative treatments of multi-walled carbon nanotubes on their electrocatalytic properties. Electrochim Acta 62:163–171. https://doi.org/10.1016/j.electacta.2011.12.043

[48] Yang K, Han H, Pan X et al (2008) The effect of chemical treatment on the crystallinity of multi-walled carbon nanotubes. J Phys Chem Solids 69:222–229. https://doi.org/10.1016/j.jpcs.2007.08.069

[49] Wepasnick KA, Smith BA, Schrote KE et al (2011) Surface and structural characterization of multi-walled carbon nanotubes following different oxidative treatments. Carbon N Y 49:24–36. https://doi.org/10.1016/j.carbon.2010.08.034

[50] Wang L, Feng S, Zhao J et al (2010) A facile method to modify carbon nanotubes with nitro/amino groups. Appl Surf Sci 256:6060–6064. https://doi.org/10.1016/j.apsusc.2010.03.120

[51] Wang Y, Malhotra SV, Owens FJ, Iqbal Z (2005) Electrochemical nitration of single-wall carbon nanotubes. Chem Phys Lett 407:68–72. https://doi.org/10.1016/j.cplett.2005.03.050

[52] Olivares F, Segura del Río R, Reyes J et al (2021) Enhanced photoconversion efficiency of hybrid TiO_2/nox-MWCNT/Si

photoanode for water splitting in neutral medium. Mater Lett 285:129128. https://doi.org/10.1016/j.matlet.2020.129128

[53] Cárdenas-Triviño G, Segura RA, Reyes-Gasga J (2004) Palladium nanoparticles from solvated atoms—stability and HRTEM characterization. Colloid Polym Sci 282:1206–1212. https://doi.org/10.1007/s00396-004-1060-0

[54] Segura RA, Hevia S, Häberle P (2011) Growth of carbon nanostructures using a Pd-based catalyst. J Nanosci Nanotechnol 11:10036–10046. https://doi.org/10.1166/jnn.2011.4998

[55] Esquivel-Peña V, Bastos-Arrieta J, Muñoz M et al (2019) Metal nanoparticle–carbon nanotubes hybrid catalysts immobilized in a polymeric membrane for the reduction of 4-nitrophenol. SN Appl Sci 1:347. https://doi.org/10.1007/s42452-019-0357-z

[56] Datsyuk V, Kalyva M, Papagelis K et al (2008) Chemical oxidation of multiwalled carbon nanotubes. Carbon N Y 46:833–840. https://doi.org/10.1016/j.carbon.2008.02.012

[57] He G, Li X, Jiang Y et al (2020) Bioinspired hierarchical interface design for improved mechanical and safety properties in energetic polymer composites. J Mater Sci 55:15726–15740. https://doi.org/10.1007/s10853-020-05130-3

[58] Bekyarova E, Itkis ME, Ramesh P et al (2009) Chemical modification of epitaxial graphene: spontaneous grafting of aryl groups. J Am Chem Soc 131:1336–1337. https://doi.org/10.1021/ja8057327

[59] Kolanowska A, Wa P, Zie W et al (2019) Selective carboxylation versus layer-by-layer unsheathing of multi-walled carbon nanotubes: new insights from the reaction with boiling nitrating mixture †. RSC Adv 9:37608–37613. https://doi.org/10.1039/c9ra08300f

[60] Santangelo S, Messina G, Faggio G et al (2012) Effect of sulphuric-nitric acid mixture composition on surface chemistry and structural evolution of liquid-phase oxidised carbon nanotubes. J Raman Spectrosc 43:1432–1442. https://doi.org/10.1002/jrs.4097

[61] Saito R, Hofmann M, Dresselhaus G et al (2011) Raman spectroscopy of graphene and carbon nanotubes. Adv Phys 60:413–550. https://doi.org/10.1080/00018732.2011.582251

[62] Kolanowska A, Wasik P, Zięba W, Terzyk AP (2019) Selective carboxylation: versus layer-by-layer unsheathing of multi-walled carbon nanotubes: new insights from the reaction with boiling nitrating mixture. RSC Adv 9:37608–37613. https://doi.org/10.1039/c9ra08300f

[63] Dresselhaus MS, Dresselhaus G, Saito R, Jorio A (2005) Raman spectroscopy of carbon nanotubes. Phys Rep 409:47–99. https://doi.org/10.1016/j.physrep.2004.10.006

[64] Gogoi D, Namdeo A, Golder AK, Peela NR (2020) Ag-doped TiO2 photocatalysts with effective charge transfer for highly efficient hydrogen production through water splitting. Int J Hydrogen Energy 45:2729–2744. https://doi.org/10.1016/j.ijhydene.2019.11.127

[65] Yao Y, Li G, Ciston S et al (2008) Photoreactive TiO2/carbon nanotube composites: synthesis and reactivity. Environ Sci Technol 42:4952–4957. https://doi.org/10.1021/es800191n

[66] Ahn JY, Kim JHJH, Moon KJ et al (2013) Incorporation of multiwalled carbon nanotubes into TiO2 nanowires for enhancing photovoltaic performance of dye-sensitized solar cells via highly efficient electron transfer. Sol Energy 92:41–46. https://doi.org/10.1016/j.solener.2013.02.031

[67] Makuła P, Pacia M, Macyk W (2018) How to correctly determine the band gap energy of modified semiconductor photocatalysts based on UV–Vis spectra. J Phys Chem Lett 9:6814–6817. https://doi.org/10.1021/acs.jpclett.8b02892